Electronic Supplementary Information (ESI)

Light concentration and electron transfer effects in plasmonic–photonic Ag, Au modified Mo-BiVO₄ inverse opal photoelectocatalysts

Martha Pylarinou,[a] Elias Sakellis,[a, b] Polychronis Tsipas,[b] Spiros Gardelis,[a] Vassilis Psycharis,[b] Athanasios Dimoulas,[b] Thomas Stergiopoulos[b] and Vlassis Likodimos*[a]

[a] Section of Condensed Matter Physics, Department of Physics, National and Kapodistrian University of Athens, University Campus, 15784, Greece. E-mail: vlikodimos@phys.uoa.gr
[b] Institute of Nanoscience and Nanotechnology, National Center for Scientific Research "Demokritos", 15341 Agia Paraskevi, Athens, Greece

S1 Materials Characterization

The films morphology and phase composition were characterized using a FEI Quanta Inspect scanning electron microscope (SEM) coupled with energy-dispersive X-ray analyzer (EDX) and a FEI Talos F200i scanning transmission electron microscope (TEM) operating at 200 keV, equipped with a windowless energy-dispersive spectroscopy microanalyzer (6T/100 Bruker). The films structural properties were studied by X-ray powder diffraction (XRD) and micro-Raman spectroscopy. XRD data were collected with a SmartLab Rigaku θ/θ Bragg-Brentano Rigaku diffractometer, equipped with a pyrolytic graphite monochromator at diffracted beam position and using Cu Kα radiation. The power conditions were set at 40 kV/35 mA and the aperture slits were set at 2/3°, 2/3°, 0.6°. The continuous step-scanning technique was used at steps of 0.03° with measuring time of 11 s/step and the recorded 2 θ range was from 15 to 55°. Micro-Raman spectra were acquired using an inVia Reflex microscope by means of a ×50 (NA=0.75) objective with 785 nm laser excitation at low power density (0.1 mW/μm²) to avoid local heating by the laser beam. X-ray photoelectron spectroscopy (XPS) was performed on PHOIBOS 100 (SPECS) hemispherical analyzer using Mg-Kα (1253.6 eV) X-ray source. The spectrometer was calibrated on clean Ag, Cu, and Au samples for which the Ag $3d_{5/2}$, Cu $2p_{3/2}$, and Au $4f_{7/2}$ peak positions were determined at 368.3, 932.7, and 84 eV, respectively. The XPS spectra were collected at a 52° take-off angle using a pass energy of 7 eV. The adventitious C 1s set to 284.8 eV was used for charge referencing. Fitting was performed using XPS Peak Fit and Shirley background subtraction. The optical properties were investigated by diffuse and specular reflectance measurements using a fiber-optic diffuse and a 15° specular reflectance accessory on a Cary60 UV-Vis spectrometer, respectively. A Halon reference and a UV-enhanced Al mirror were used for background determination. Photoluminescence (PL) measurements were performed using FluoroMax Plus (Horiba) spectrofluorometer.

S2 Photoelectrochemical Performance

Photoelectrochemical experiments were performed in a three-electrode configuration on a CS350 potentiostat/galvanostat (Corrtest Instruments) using the PC films deposited on FTO substrates as working electrode, Ag/AgCl as reference and a Pt foil as counter electrodes in aqueous 0.5 M NaHCO₃ aqueous electrolyte. Visible light illumination was provided by a 300 W Xe lamp in combination with a 400 nm cutoff filter delivering 100 mW/cm² at the

photoelectrode surface. Linear sweep voltammetry was performed at a potential scan rate of 10 mV s^{-1} under dark conditions and back side visible light illumination. The applied potential vs. Ag/AgCl was converted to reversible hydrogen electrode (RHE) scale by using equation

$$E_{RHE} = E_{Ag/AgCl} + 0.059 \text{ pH} + E^0_{Ag/AgCl}.$$

where $E^0_{Ag/AgCl} = 0.1976$ V is the standard potential for Ag/AgCl at 25 °C. Electrochemical impedance spectroscopy (EIS) was performed at open-circuit voltage, in the 10^4–10^{-2} Hz frequency range with ac amplitude of 10 mV.

Incident photon-to-current efficiency (IPCE) measurements were also performed in 0.5 M NaHCO$_3$ aqueous electrolyte under back-side illumination at 1.23 V vs RHE potential using a 1 kW Xe lamp in combination with an Oriel 77200 1/4 monochromator and a calibrated Si photodiode. IPCE was calculated according to the following relation:

$$IPCE\ (\%) = \frac{1239.8\ [\text{V nm}] \times J[\text{mA/cm}^2]}{\lambda[\text{nm}] \times P[\text{mW/cm}^2]} \times 100\ \%$$

where J is the photocurrent density in mA/cm^2, λ is the wavelength of incident light in nm, and P is the monochromatic light power density (mW/cm^2).

Photoelectrocatalytic experiments were also carried out in three-electrode configuration using a 300 W Xe lamp in combination with a 400 nm long-pass filter (100 mW/cm^2) using 36 ml working solution of 0.1 M NaHCO$_3$ supporting electrolyte under mild stirring, comprising 22 mg/L of tetracycline and 7 mg/L ibuprofen pharmaceutical pollutants. Degradation kinetics was monitored by spectrophotometric detection for small aliquots periodically withdrawn from the reaction cell. The degradation tests were performed in triplicate, and standard errors were calculated for the mean kinetic constants. Additional TC and IBU photoelectrocatalytic tests were carried out in the presence of 5 mM isopropanol (IPA) and formic acid (FA) as well as 1 mM 1,4 benzoquinone (BQ) as hydroxyl radical, hole and superoxide radical anion scavengers, respectively.
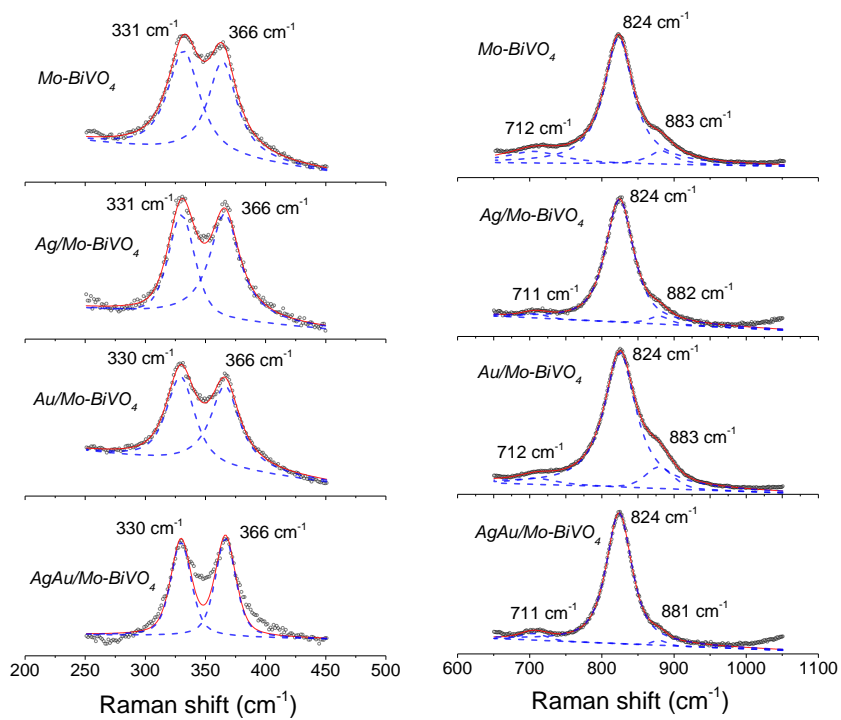
Fig. S1 Spectral deconvolution (solid-dashed lines) of the bending (left) and stretching (right) VO_4 vibrational modes from the corresponding Raman spectra (open circles) for the single-, Ag-, Au- and (Ag,Au)-modified Mo BiVO$_4$ PC340 films.
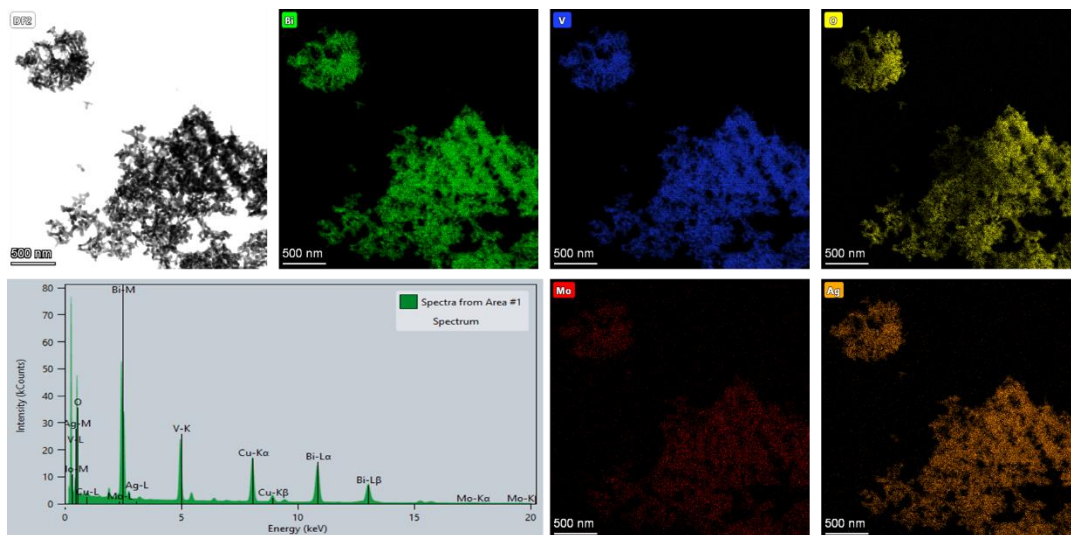
Fig. S2 TEM image of Ag/Mo-BiVO₄ PC340 films and the corresponding Bi, V, O, Mo, and Ag elemental maps obtained from the corresponding local EDX spectra.
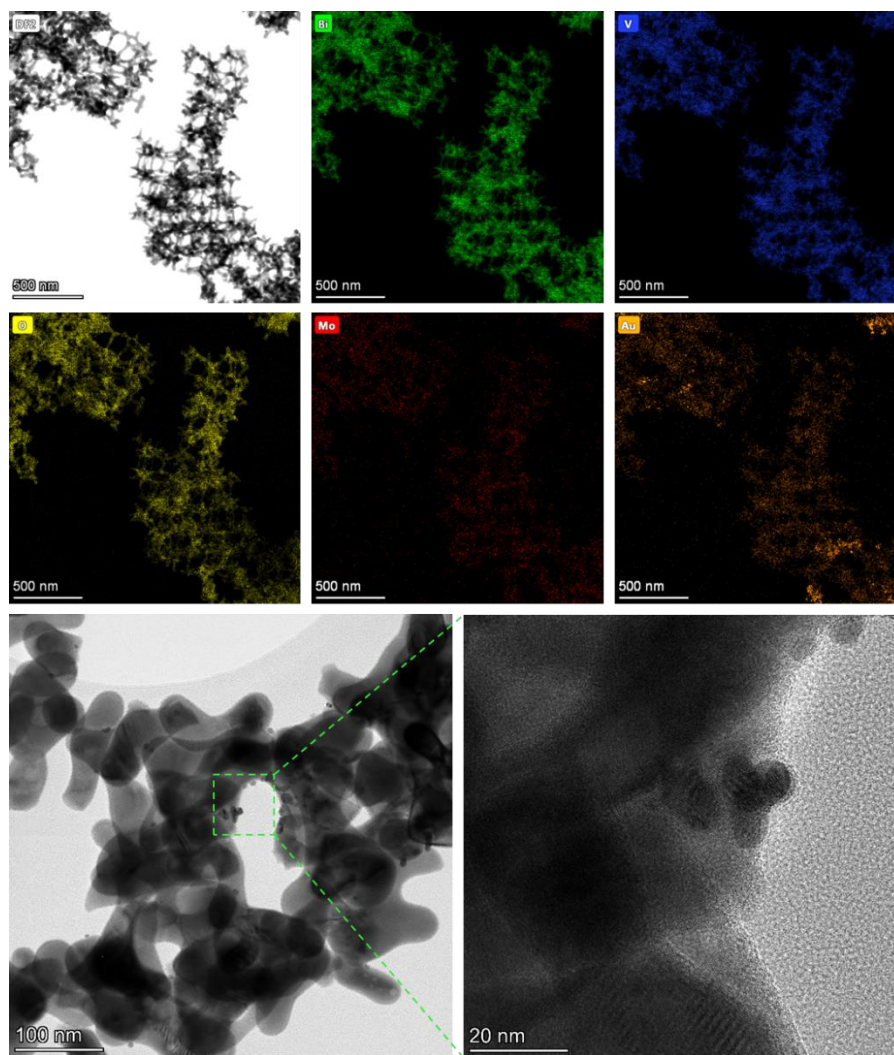
Fig. S3 (Upper and middle panels) TEM image of Au/Mo-BiVO$_4$ PC340 films and the corresponding Bi, V, O, Mo, and Au elemental maps. (Bottom panel) TEM images at higher magnification showing the presence of Au NP aggregates decorating the large BiVO$_4$ nanocrystals.
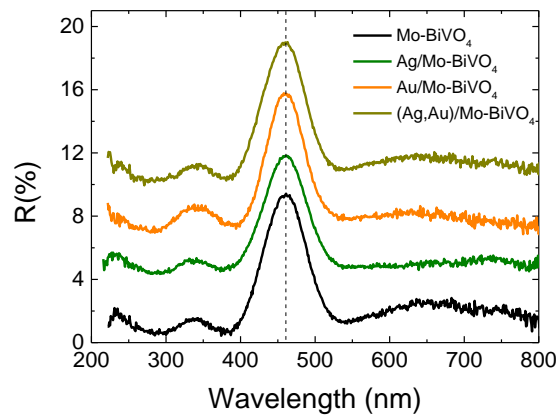
Fig. S4 Specular reflectance (R%) at 15° incidence angle for the Ag and Au-modified Mo-BiVO$_4$ PC340 films.
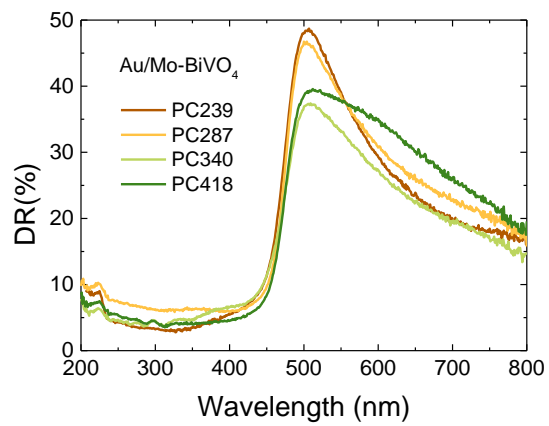

Fig. S5 Diffuse reflectance (R%) at 15° incidence angle for the Au-modified Mo-BiVO$_4$ PC films.
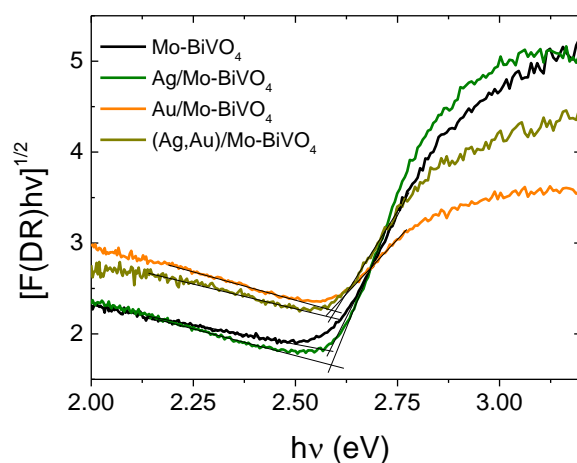
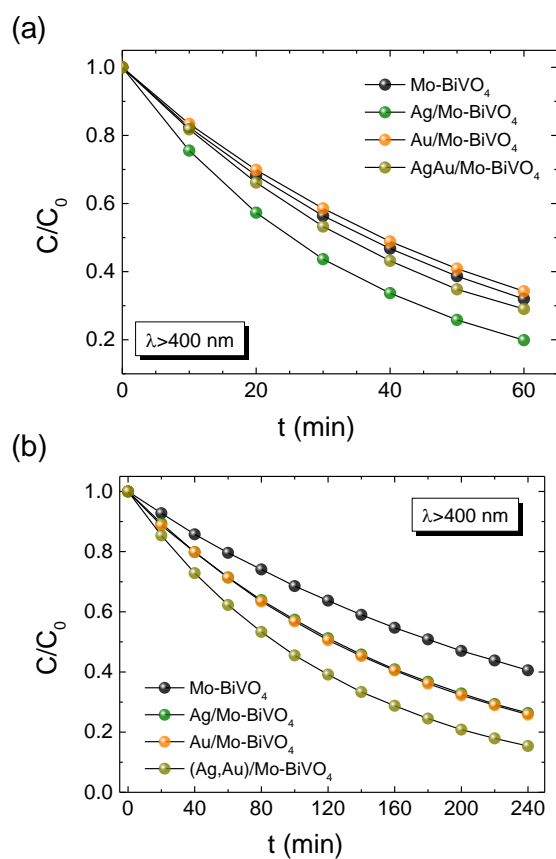**Fig. S6** Indirect band gap Tauc plots for the Ag, Au-modified Mo-BiVO$_4$ PC films.

Fig. S7 (a) TC and (b) IBU photodegradation kinetics for the Ag, Au-modified Mo-BiVO$_4$ PC340 photoelectrodes at +1.0 V vs Ag/AgCl under visible light.
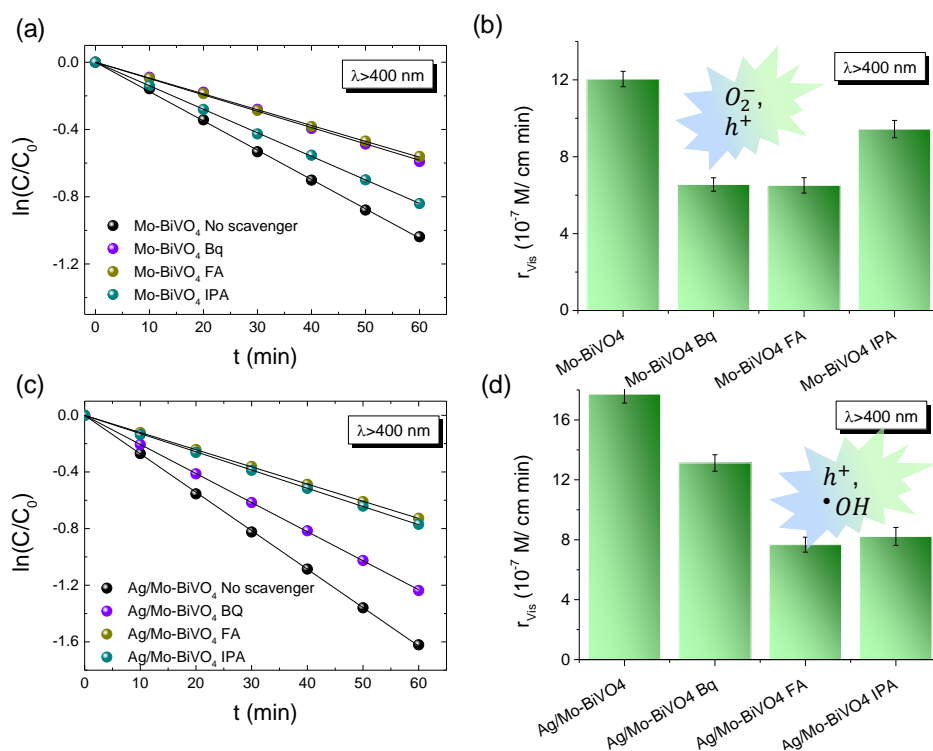
Fig. S8 TC photoelectrocatalytic degradation kinetics and the corresponding reaction rates r_{vis} for (a), (b) Mo-BiVO$_4$ and (c), (d) Ag/Mo-BiVO$_4$ PC340 films in the presence of Bq, FA and IPA radical scavengers in 0.1 M NaHCO$_3$ supporting electrolyte at applied potential of +1.0 V vs Ag/AgCl under visible light.
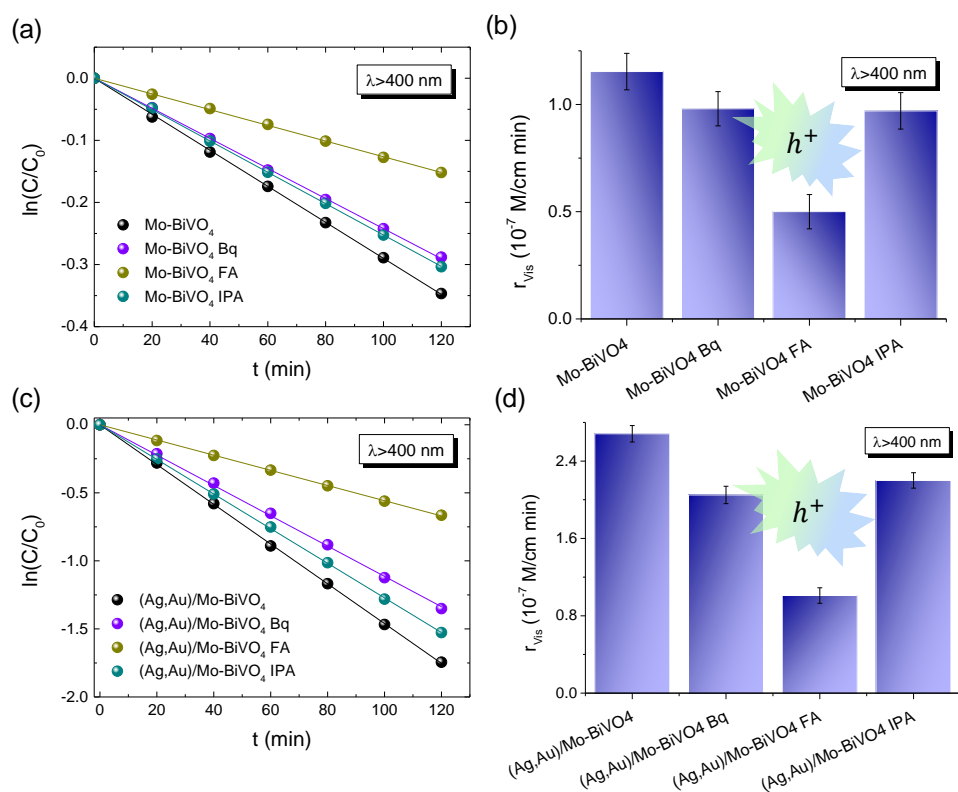
Fig. S9 IBU photoelectrocatalytic degradation kinetics and the corresponding reaction rates r_{vis} for (a), (b) Mo-BiVO$_4$ and (c), (d) (Ag,Au)/Mo-BiVO$_4$ PC340 films in the presence of Bq, FA and IPA radical scavengers in 0.1 M NaHCO$_3$ supporting electrolyte at applied potential of +1.0 V vs Ag/AgCl under visible light.
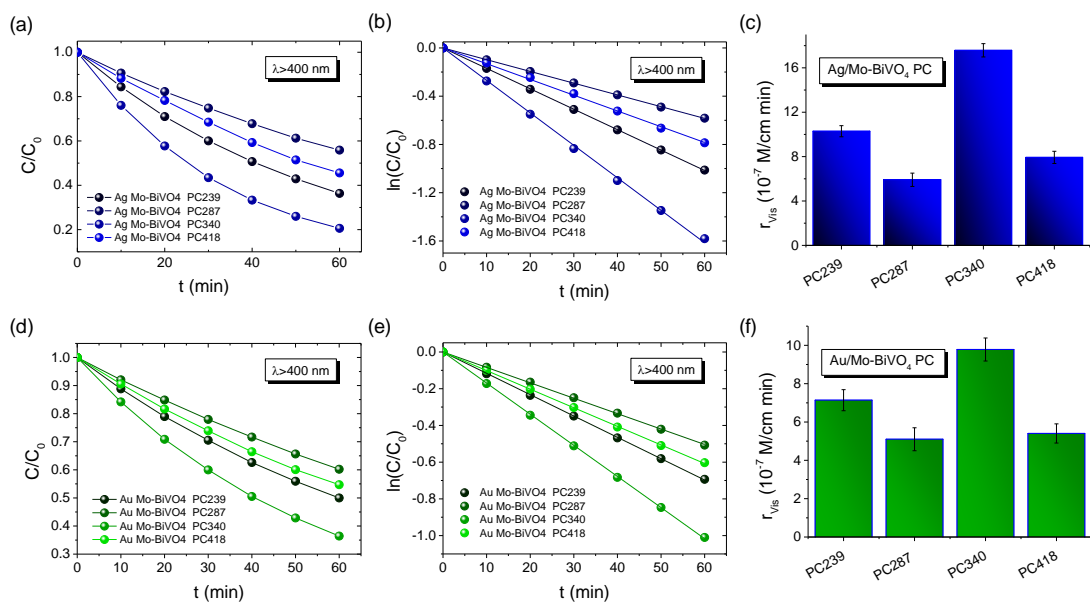
Fig. S10 TC photodegradation kinetics and reaction rates for the Ag- and Au-modified Mo-BiVO₄ PC films in 0.1 M NaHCO₃ supporting electrolyte at +1.0 V vs Ag/AgCl under visible light irradiation as a function of the PC macropore diameter.
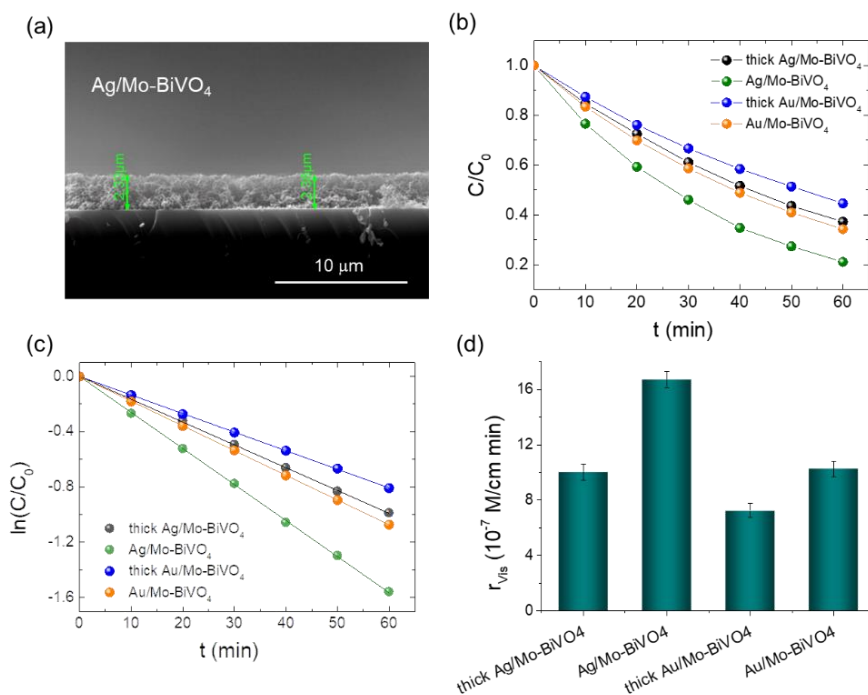
Fig. S11 (a) Cross section SEM image of the thick Ag/Mo-BiVO$_4$ film. (b)-(d) Comparative TC photodegradation kinetics and reaction rates for the thick and thin (pristine) Ag- and Au-modified Mo-BiVO$_4$ PC films in 0.1 M NaHCO$_3$ supporting electrolyte at +1.0 V vs Ag/AgCl under visible light irradiation.
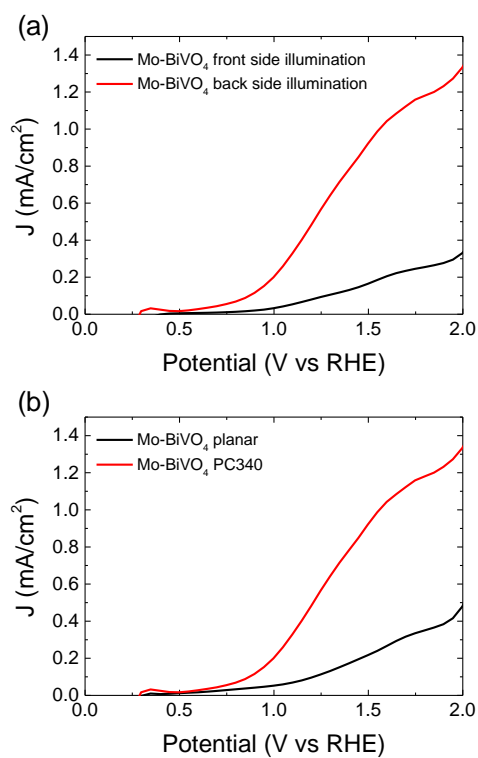
Fig. S12 (a) Current density-potential curves of Mo-BiVO$_4$ PC340 films under front and back side visible light illumination. (b) Current density-potential curves for planar and Mo-BiVO$_4$ PC340 films under back side visible light illumination. All measurements are carried out in 0.5 M NaHCO$_3$ aqueous electrolyte.
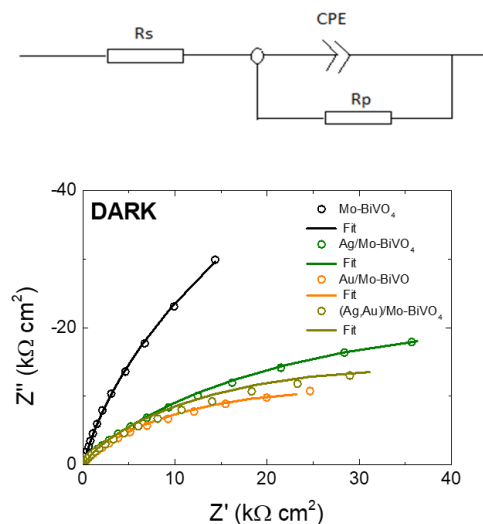
Fig. S13. EIS Nyquist plots for the Ag and Au-modified Mo-BiVO$_4$ PC340 films under dark conditions. Solid lines depict the best fit curves to the modified Randles equivalent circuit (top scheme).
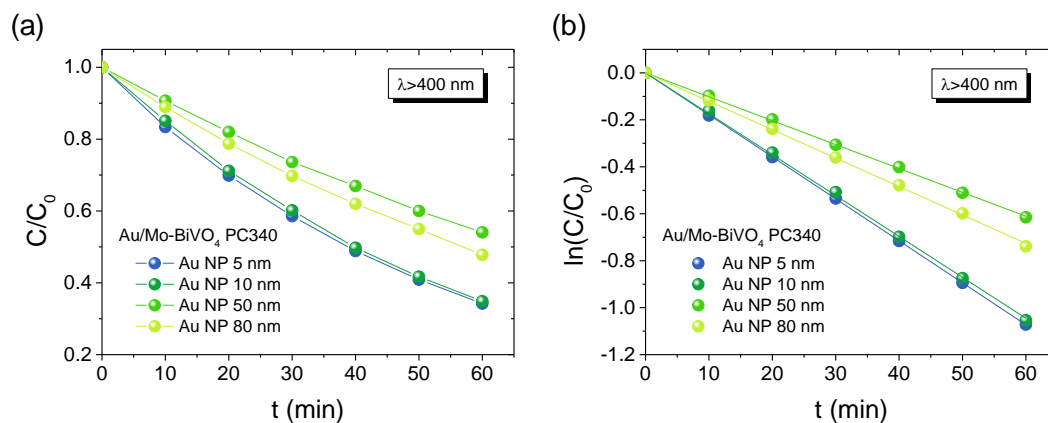

Fig. S14 TC photodegradation kinetics for the Au/Mo-BiVO$_4$ PC340 photoelectrodes with Au NPs of different diameters (5, 10, 50 and 80 nm) in 0.1 M NaHCO$_3$ supporting electrolyte at +1.0 V vs Ag/AgCl under visible light.
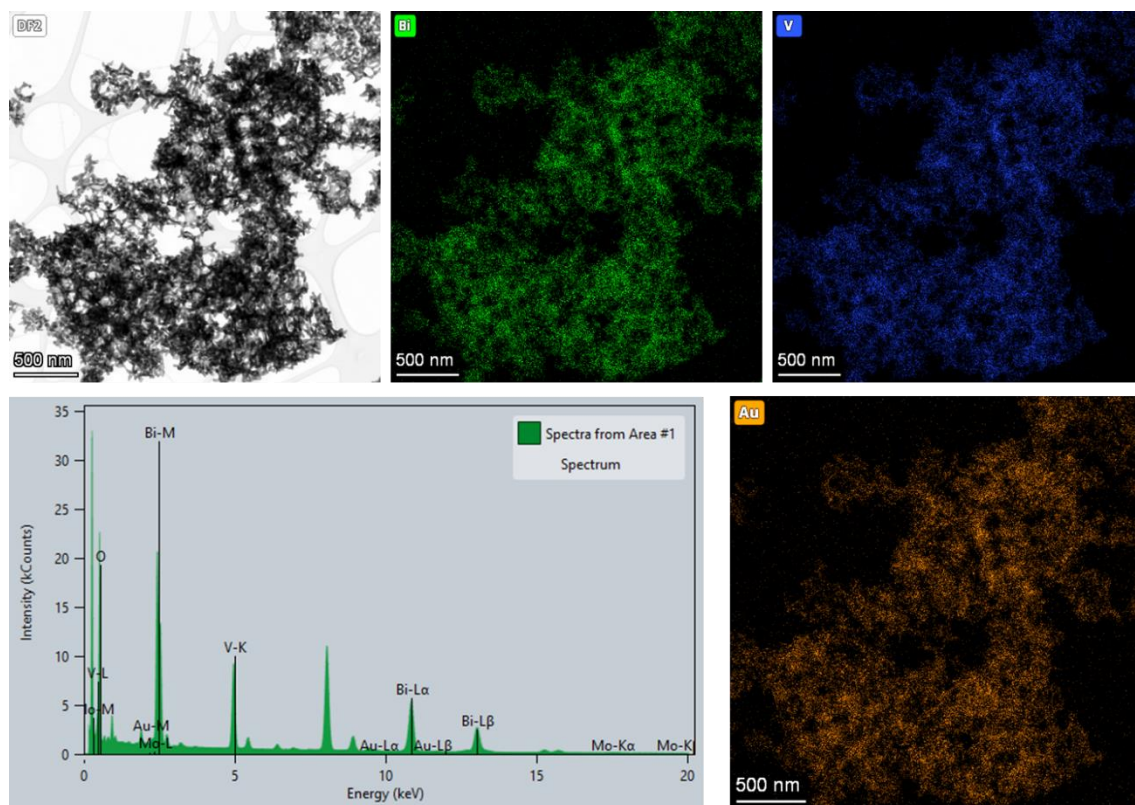
Fig. S15 TEM image of 10 nm Au/Mo-BiVO$_4$ PC340 films and the corresponding Bi, V and Au elemental maps obtained from the corresponding local EDX spectra.
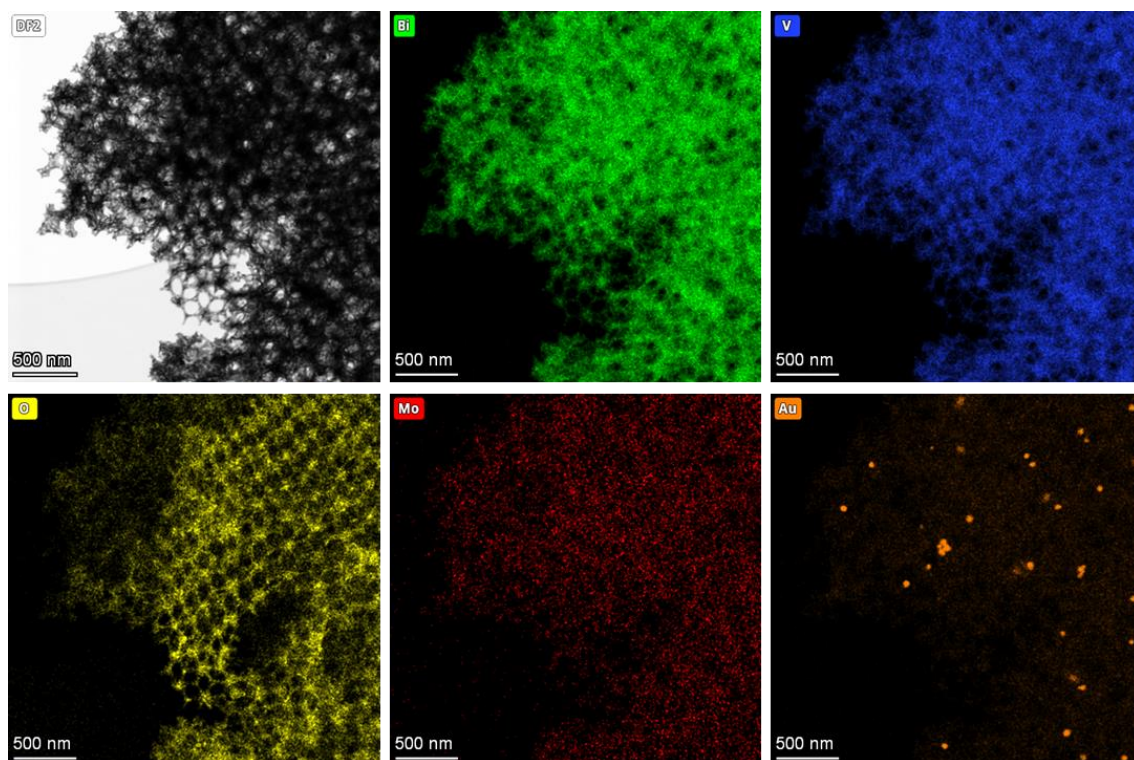
Fig. S16 TEM image of 50 nm Au/Mo-BiVO$_4$ PC340 films and the corresponding Bi, V, O, Mo, and Au elemental maps.
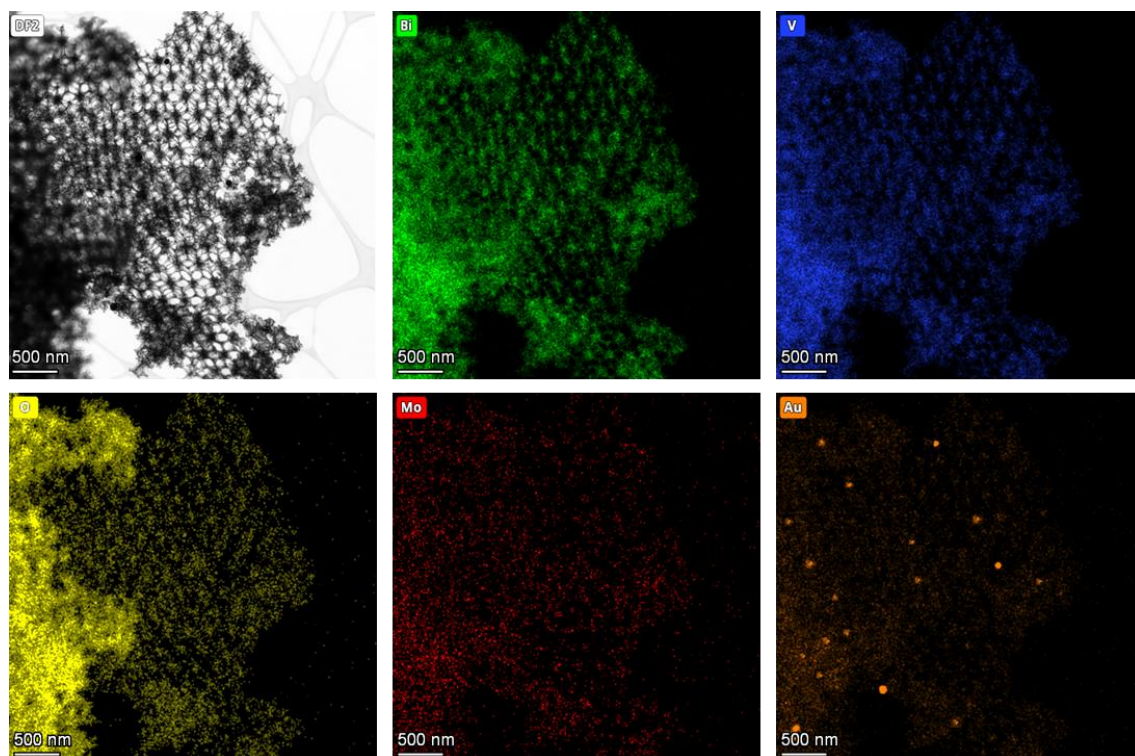
Fig. S17 TEM image of 80 nm Au/Mo-BiVO$_4$ PC340 films and the corresponding Bi, V, O, Mo, and Au elemental maps.

Table S1. Structural and optical parameters for the BiVO$_4$ PC films.

Film	D (nm)	$\lambda_{\exp}$ (15°) (air)	n_{eff} (air)	$1-f$	λ (0°) (air)	n_{eff} (H$_2$O)	λ (0°) (H$_2$O)
PC239	165	382	1,44	0,226	388	1,63	440
PC287	185	413	1,39	0,197	420	1,60	483
PC340	210	462	1,37	0,185	470	1,58	543
PC418	260	534	1,28	0,136	545	1,52	646

D = inverse opal macropore diameter determined from SEM.
$\lambda_{\exp}$ (15°) = stop band wavelength determined from R% spectra at 15° incidence.
λ (0°) = stop band wavelength according to the modified Bragg law at 0° incidence.

The stop band positions were estimated by modified Bragg's law for first order diffraction from the (111) *fcc* planes: $\lambda = 2d_{111}\sqrt{n_{eff}^2 - \sin^2\theta}$, where λ is the stop band wavelength, $d_{111} = \sqrt{2/3}\,D$ is the interplanar spacing of (111) planes, D is the macropore diameter and $n_{eff}^2 = n_{sphere}^2 f + n_{BiVO_4}^2(1-f)$ is the volume-weighted average of the spheres' refractive index, n_{sphere}, and bismuth vanadate, n_{BiVO_4}, occupying the inverse opal skeleton, with f being the solid filling fraction ($f = 0.74$ for the *fcc* lattice) and θ being the angle between the incident beam and the plane normal. Using the experimental stop band wavelengths at $\theta = 15°$ along with the measured diameters for $n_{BiVO_4} = 2.4$ and $n_{air} = 1.0$, the n_{eff} values and filling fraction $1-f$ was determined in air. In addition, using the obtained filling fractions and $n_{H_2O} = 1.33$, the stop band position was estimated for the PC films in water, as reported in the manuscript text.

Table S2. Parameters obtained by fitting the experimental impedance spectra to a modified Randles circuit.

PC film	Dark		Visible light (>400 nm)		UV-vis	
	R_S	R_{CT}	R_S	R_{CT}	R_S	R_{CT}
	(Ω)	(Ω)	(Ω)	(Ω)	(Ω)	(Ω)
Mo-BiVO$_4$	11.9	2.23×10^5	13.1	7292	12.1	4974
Ag/Mo-BiVO$_4$	11.0	0.54×10^5	10.7	5968	11.4	3254
Au/Mo-BiVO$_4$	9.3	0.28×10^5	9.3	5733	8.9	2536
(Ag,Au)/Mo-BiVO$_4$	10.4	0.35×10^5	10.4	5455	10.3	2122